Beam shaping by volume phase structures in photo-thermo-refractive glass

Marc SeGall*, Ivan Divliansky, Daniel Ott, Julien Lumeau, Sergiy Mokhov, Boris Zeldovich, and Leonid B. Glebov
CREOL – The College of Optics & Photonics, University of Central Florida, P.O. Box 162700
Orlando, FL USA 32816-2700

Keywords: phase mask, beam shaping, mode conversion, aberration correction

ABSTRACT

We demonstrate the recording of volume phase masks in the bulk of photo-thermo-refractive glass. Recording was produced by exposing the glass to UV radiation through binary amplitude masks. Depending on the profile of the amplitude mask either a binary volume phase mask or a grayscale phase mask may be produced. Volume phase masks have been used to generate Fresnel lenses, convert a Gaussian beam into higher order Hermite-Gauss and Laguerre-Gauss modes, to produce optical vortices, and to create aberration-correcting optical components.

Phase masks have been used for decades for a variety of applications, including improving the depth of field [1-3], manufacture of electronics [4], encryption [5-8], and coronagraphy [9-11]. Conventional fixed phase masks are generally produced by either sculpting the surface of a thin film such as PMMA or by recording it in the bulk of a photosensitive material such as DCG or lithium niobate. Active phase masks may also be produced using spatial light modulators. In either case these masks may be used effectively in low power systems as they can be designed to have nearly any phase profile. However, such elements have several drawbacks as well. Absorption in these materials prevents them from being used in high power systems, and thin film and SLM phase masks may also be damaged from mishandling or by placement in high temperature conditions. In order to have a robust phase mask suitable for use in such systems it is therefore necessary to utilize a low-absorption substrate with the phase mask recorded in the bulk to prevent damage via mishandling. Here we present a method for recording volume phase masks (VPMs) in the bulk of photo-thermo-refractive (PTR) glass.

PTR glass is a sodium-potassium-zinc-aluminum-fluorine-bromine-silicate glass doped with cerium, antimony, tin, and silver, with a region of transparency from 350 nm to 2700 nm and a damage threshold of 40 J/cm^2 [12, 13]. Due to this wide transparency window, PTR glass is used to produce volume Bragg gratings for the visible and infrared regions, which have found applications in pulse stretching and compression [14], beam combining [15,16], and ultra-narrow spectral filtering [17,18]. In the near IR region PTR glass has an absorption coefficient of ~10^{-4} cm^{-1}, which, coupled with its glass transition temperature of ~460^{o}C [12], makes a suitable substrate for high power and high temperature systems. In addition, forced air cooling can be applied to the sample without degrading the recorded profile or seriously

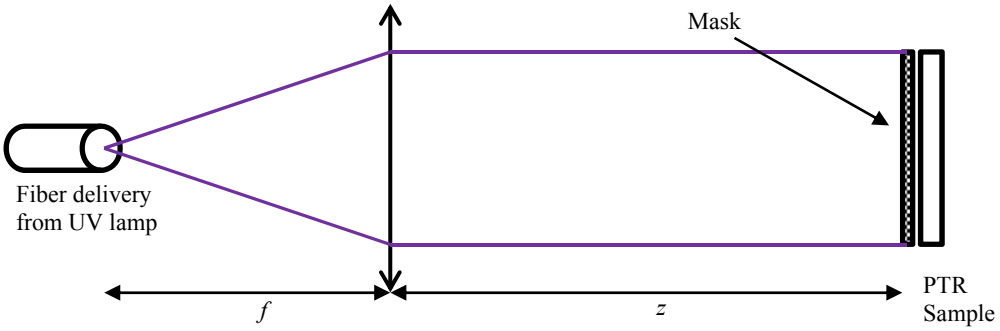

Fig. 1: Recording geometry for producing a phase mask using the contact-copy technique.

Laser Beam Shaping XIV, edited by Andrew Forbes, Todd E. Lizotte, Proc. of SPIE Vol. 8843, 884307

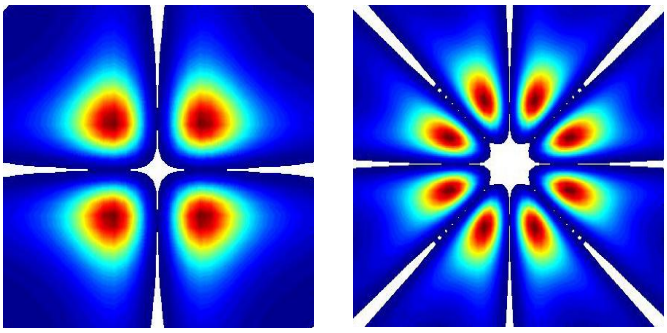

(a) (b)

Fig. 2: (Color online) Simulated far field intensity distributions produced by the four sector (a) and eight-sector (b) phase masks.

affecting the transmitted beam [19]. Here we record phase masks in the bulk of the glass by utilizing the contact-copy method and a specialized amplitude mask.

The contact-copy method, shown in Fig. 1, places an amplitude mask in direct contact with a PTR sample and the combined element illuminated by a UV source. Binary phase masks may be produced by using binary amplitude masks which have a transmittance function matching the desired phase distribution. In the literature binary phase masks have been used in applications such as coronagraphy [9-11] and mode conversion [20]. To investigate whether binary VPMs can achieve the same conversion efficiency as traditional phase masks when converting a Gaussian beam to higher order modes two mode-converting phase masks are considered here. The first mask contains four sectors, designed to convert a Gaussian to the TEM_{11} mode, and the second mask contains eight, designed to convert the beam to the LG_{04} mode. Each sector in the masks has a π phase shift relative to its neighbors. In both cases when a Gaussian beam is incident upon the mask, after acquiring the local phase change it is no longer a pure Gaussian beam. Therefore it can be described as a superposition of a Gaussian beam with higher order Hermite-Gauss modes or Laguerre-Gauss modes as each set of modes represents a basis for which any field distribution can be described. The conversion efficiency of the phase mask from a Gaussian to a given higher order mode is equal to the fraction of power that is transferred from the Gaussian mode that higher order mode. Note however that because higher order modes have a different energy distribution than a Gaussian beam, the size of the bucket containing a given amount of energy will be different for a higher mode than a Gaussian beam assuming the same beam radius. Therefore the conversion efficiency of the phase masks will depend on the relative sizes of the beams. Simulations of ideal binary phase masks indicate that the maximum conversion efficiency of a Gaussian into the TEM_{11} mode using a binary phase mask is 68.4% and the maximum conversion efficiency into the LG_{04} mode is 29% [21]. In the far field these binary masks will produce the intensity distributions shown in Fig. 2.

In order to verify these simulations we fabricated the described masks using a 1.1 mm He-Cd beam at 325 nm using a raster scan to illuminate the entire profile. After thermal development the refractive index change was measured using a custom shearing interferometer [22]. The refractive index change of 208 ppm and 175 ppm was measured for the four-sector and eight-sector mask, respectively. They were then polished to 1.52 mm and 1.81 mm, respectively, in order to achieve a π phase shift at 633 nm. As shown in Fig. 3 there is excellent agreement between the experimental and

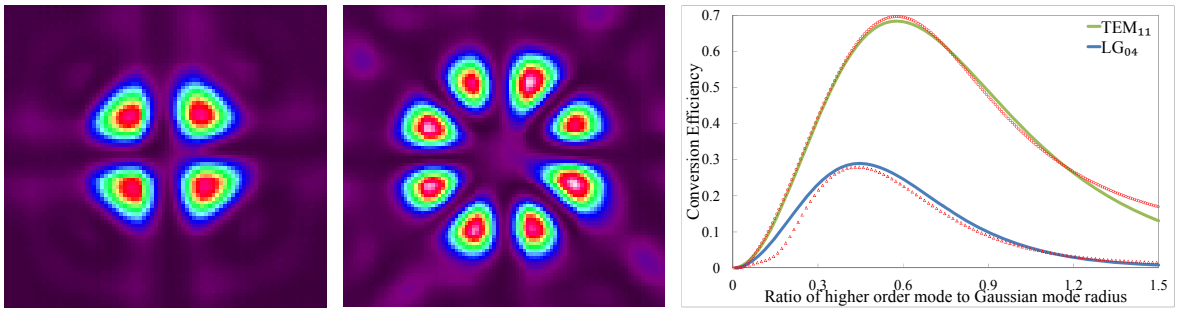

(a) (b) (c)

Fig 3: (Color online) Experimental far field profile produced by the four-sector mask (a) and eight-sector mask (b) and the conversion efficiency of these masks into their respective modes (c). Solid lines – theoretical conversion efficiency, dotted lines – experimental conversion efficiency.

theoretical far field profiles. The conversion efficiencies were measured for a variety of beam sizes and as shown in Fig. 3c there is fairly good agreement with the theoretical conversion efficiencies. Thus binary VPMs may be used as mode-converting elements.

While binary phase masks can be used in various applications they are however limited by their binary nature. In order to create grayscale phase masks a different type of amplitude mask must be used. In the ideal case the new mask is a grayscale amplitude mask, with an amplitude profile matching the desired phase profile. Grayscale amplitude masks however are much more expensive than standard chrome-on-silica masks, making them an impractical choice for most research. To avoid this costliness consider the case where a standard binary amplitude mask is used. The phase profile recorded in the PTR sample will be the Fresnel diffraction pattern of this mask. Because the PTR sample is thick, (upwards of several millimeters) diffraction from the amplitude mask will result in sharp edges being washed out. If a given aperture is very small (on the order of a micron) then diffraction effects will be severe, with the region surrounding the aperture receiving approximately the same exposure dosage as the aperture itself. By proper positioning and density of opaque and transparent apertures it is therefore possible to create a quasi-grayscale phase distribution in the PTR glass using a binary amplitude mask. This is the key to producing grayscale phase masks without resorting to expensive grayscale amplitude masks.

To produce a grayscale phase mask suppose that the desired phase profile is $\varphi(x,y)$. This profile must be converted to an amplitude profile and must therefore be normalized such that the phase distribution lies between zero and one. This profile is the profile that is necessary for a grayscale amplitude mask, and the transmitted field distribution that illuminates the PTR sample would be the Fresnel diffraction pattern of the amplitude transmittance (the square root of the intensity transmittance) of the mask. To replicate this field distribution with a binary amplitude mask, which has the same intensity transmittance and amplitude transmittance, it is necessary to take the square root of the normalized phase profile. This new profile is then pixelated and an array of random numbers between 0 and 1 is created. If a given pixel in the digitized phase array is larger than its corresponding random number the matching pixel in the amplitude mask is made opaque, and if is less than the random number it is made transparent. Therefore the probability that a given pixel is opaque or transparent in the binary amplitude mask is equal to the local normalized phase, and the average number of pixels in a region which are opaque will be approximately equal to the local normalized phase. We will henceforth refer to this type of amplitude mask as a probabilistic mask.

To demonstrate the feasibility of probabilistic masks creating volume phase masks consider the spiral phase mask. Spiral phase masks are used to produce optical vortices, which are used in applications including optical tweezers [23] and quantum cryptography [24]. A vortex exists in a beam if there is a phase singularity in the center of the beam and the beam carries orbital angular momentum. In such a case the beam intensity will be zero at the location of the singularity, and its equiphase surface is not planar but rather spirals about the optical axis. This results in an annular beam distribution which in the far field can be approximated using the Laguerre-Gaussian modes [25]:

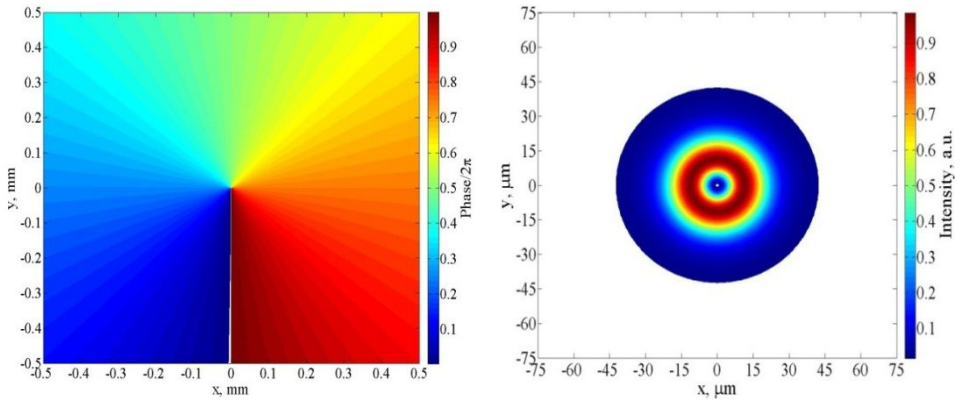

(a) (b)

Fig. 4: (Color online) Ideal phase distribution of an $m = 1$ spiral phase mask (a) and the resulting far field intensity distribution after being focused by a 100 mm lens (b).

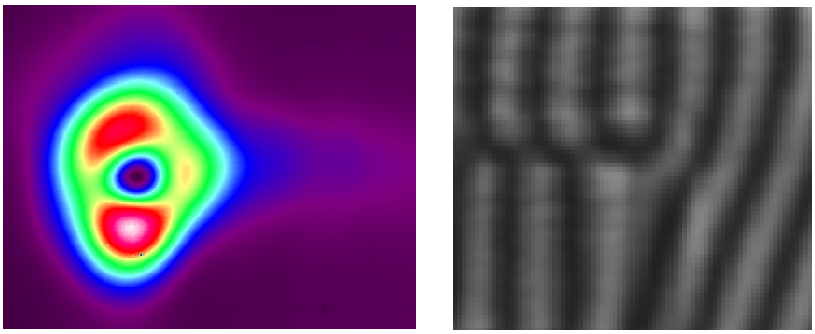

(a) (b)

Fig. 5: (Color online) Far field intensity distribution produced by a probabilistic mask (a) and the fork dislocation produced by the mask in a double-pass interferometer (b).

$$E_{nm}(r,\varphi,z) = E_0 \frac{w_0}{w(z)}\left(\frac{\sqrt{2}r}{w(z)}\right)^{|m|} L_n^{|m|}\left(\frac{2r^2}{w^2(z)}\right) e^{\frac{-r^2}{w^2(z)}} e^{im\varphi} e^{-i\left(kz-(1+2n+|m|)\arctan\left(\frac{z}{z_0}\right)+k\frac{r^2}{2R(z)}\right)}. \quad (1)$$

Of importance is the topological charge m; a photon with topological charge m will have an orbital angular momentum of $m\hbar$. If the vortex beam interferes with a reference beam the fringe pattern will have a fork discontinuity at the location of the phase discontinuity, with the number of tines in the fork equaling the topological charge of the vortex plus one [26].

In order to produce an optical vortex of topological charge $|m|$, the spiral phase mask induces an azimuthal phase variation from 0 to $2m\pi$, with the sign of m determined by the helicity of the phase variation. For simplicity only the m = 1 case will be considered here. This produces a phase profile with a line discontinuity throughout half of the phase profile, as seen in Fig. 4a, and creates an annular beam in the far field, shown in Fig. 4b, with 94% of the energy contained within the annulus. Here the edge of the annulus is defined as a 3% signal-to-noise ratio. After finding the outermost points along each axis which satisfies this condition the total energy in the annulus is calculated via a square which contains these outermost points to approximate a traditional detector.

To create this spiral phase mask a probabilistic amplitude mask was manufactured via e-beam lithography with a chrome-on-fused silica substrate and pixel sizes of 1 μm. The mask was then placed in contact with a PTR sample in the recording configuration shown in Fig. 1 and a 100 mm plano-convex lens was used as the collimating lens for the lamp. The mask and sample were placed approximately 300 mm behind the lens and illuminated by a broadband UV lamp in order to ensure that no interference pattern was inadvertently recorded. After exposure and thermal development the sample had a refractive index change of 364 ppm as measured by the shearing interferometer and it was subsequently polished to 1.75 mm in order to achieve a 2π phase shift at 633 nm.

As shown in Fig. 5a, after a 1 mm beam passed through the phase mask it achieved a nearly annular beam profile in the far field, along with a low energy diffraction tail. This diffraction tail is caused by the finite transition region at the line discontinuity. After measuring the beam power immediately after the sample and comparing it the energy in the ring in the far field (where an iris diaphragm was used to eliminate the diffraction tail), the fraction of energy in the annulus is 82 ± 1%. This is in fairly good agreement with the theoretical prediction after accounting for fabrication errors in the probabilistic mask. In order to verify that the beam is truly a vortex beam the phase mask was placed in a double-pass interferometer (Zygo), and as shown in Fig. 5b the phase mask produces a fork dislocation in the interferogram. Because the interferometer is a double-pass interferometer the topological charge of the mask is doubled, and so the three tines shown in Fig. 5b are expected rather than the two-tine pattern that would be observed in a single-pass interferometer. Therefore, probabilistic masks can produce optical vortices with approximately the same fidelity as a grayscale amplitude mask while being considerably cheaper and easier to fabricate.

Though a probabilistic mask can produce optical vortices with good fidelity, some energy was lost due to the finite transition region at the phase discontinuity. While spiral phase masks only have a single transition region, other profiles such as the Fresnel lens contain multiple transition regions and therefore we can reasonably expect that probabilistic masks will not be able to replicate these profiles well. Note that this is not a feature of the probabilistic mask but rather a feature of the contact copy method with a thick sample. A grayscale amplitude mask, while providing a slightly better

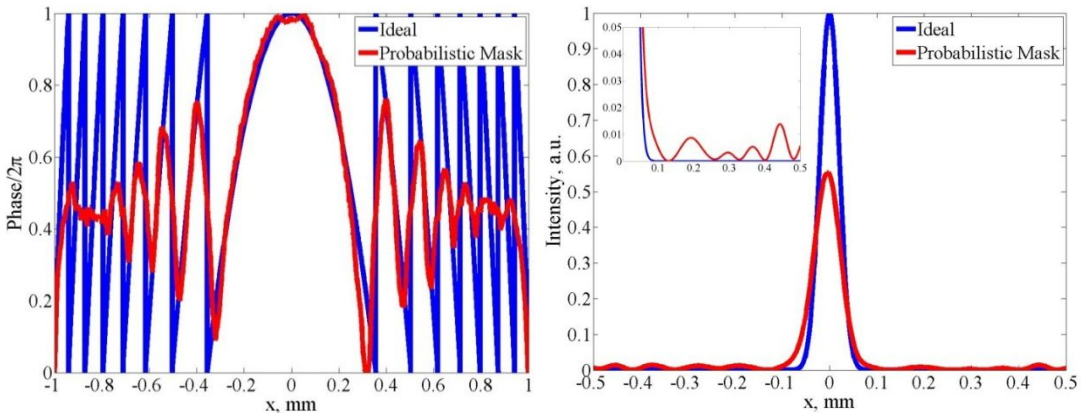

(a) (b)

Fig. 6: (Color online) Simulated phase profile of a Fresnel lens (a) and the intensity distribution in the focal plane of the lens (b).

profile than a probabilistic mask in general, will suffer from the same limitations since diffraction effects will still be present at the transition regions.

To investigate the limitations of probabilistic masks we created Fresnel lenses which replicate the phase profile of plano-convex lenses of various focal lengths. These lenses were first simulated in Matlab and as shown in Fig. 6 the probabilistic mask cannot replicate the Fresnel lens with high fidelity. As seen in Fig. 6a the recorded phase profile poorly represents the desired phase profile at the transition regions as expected, and it also has difficulty representing the smaller zones. This is because the phase profile has been digitized when creating the amplitude mask, and it is difficult to adequately sample the smaller zones without reducing the pixel size to the point where the mask would effectively be a grayscale amplitude mask. This distorted phase profile results in a degraded intensity distribution in the focal plane of the Fresnel lens, as shown in Fig. 6b. Instead of all of the energy being focused to a single spot there are low energy diffraction rings corresponding to the various transition regions. The central spot is also broader than the ideal spot.

To experimentally verify these simulations we recorded Fresnel lenses of focal lengths between 100 and 500 mm using the same recording techniques as for the spiral phase mask. Using a 1 mm beam centered on the lenses we observed a central spot which was close to Gaussian surrounded by low energy rings, as shown in Fig. 7. The focusing efficiency of the lenses was measured by measuring the power in the central spot as compared to the total transmitted power, giving an ideal Fresnel lens a diffraction efficiency of unity. The focusing efficiencies, listed in Table 1, are in excellent agreement with the simulated phase profiles. Note that in order to have a focusing efficiency larger than 90% the Fresnel lenses must have focal lengths of at least 200 mm. For larger beams where there is more power being transmitted through the smaller zones the focal length must be even longer. Thus probabilistic masks should be designed to have a minimum number of phase transitions in order to reproduce the desired phase profile with good fidelity.

Provided that the phase mask has been designed such that there are no more than a few transition regions then it may be used in any application that a traditional mask can be used. Here we consider the use of VPMs as aberration

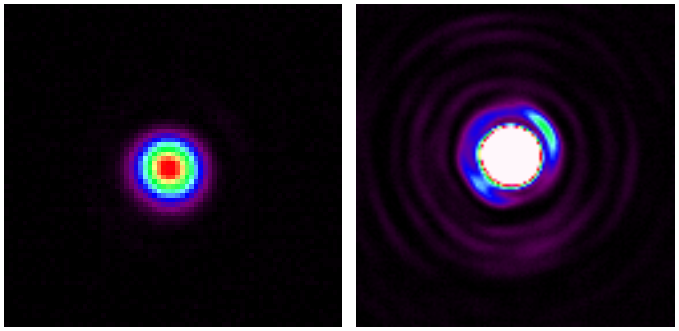

(a) (b)

Fig. 7: (Color online) Experimental intensity distribution in the focal plane of a 200 mm probabilistic Fresnel lens (a). When the intensity is increased, low energy diffraction rings become visible.

Table 1: Focusing efficiencies of probabilistic Fresnel lenses for various focal lengths.

f, mm	$\eta_{theoretical}$ (%)	$\eta_{experimental} \pm 1\%$
50	57.2	-
100	77.9	76.2
200	91.3	92.5
300	96.3	-
500	98.0	94.7

correcting elements. In a fixed system where the aberrations have been measured then a phase mask containing the opposite amount of aberrations will correct the system. Note however that placing a thick plate into a system will result in a different aberration profile [27], so in order to properly measure the aberrations of the system the PTR blank should be inserted into the system. Once steady-state has been reached the aberrations can be properly characterized. These aberrations can then be selectively adjusted with a phase mask such that the desired beam profile is achieved.

Here we developed two aberration-correcting phase masks. In the first case, a 200 mm plano-convex lens was placed in an interferometer and deliberately misaligned in order to produce a small amount of coma and astigmatism in addition to the spherical aberration. The phase mask was then designed to correct only the spherical aberration. After recording the phase mask it was developed over several steps and the aberrations measured after each step. As shown in Fig. 8a the coma and astigmatism are unchanged while the spherical aberration is eliminated. The slight change in coma and astigmatism during the last step is a result of the increased scattering caused by repeated thermal developments.

The second aberration-correcting mask was designed to alter coma and spherical aberrations while leaving astigmatism unchanged. Rather than use the Seidel description of aberrations however we used Zernike polynomials [28] and designed the phase mask to correct different amounts of coma x and coma y. Note that this mask was not designed to correct the coma and spherical aberrations of the 200 mm lens from before but rather to correct a preset amount of aberrations. As with the previous corrector this mask was developed over several stages and the amount of correction measured by treating the mask as an aberration-inducing element in an otherwise ideal system. As seen in Fig. 8b the spherical, coma x, and coma y aberrations are all altered individually while not changing the astigmatism. Therefore we are able to produce aberration-correcting elements using VPMs.

In conclusion we have demonstrated a cost-effective way to produce phase masks in a substrate suitable for use in a high power system. Binary volume phase masks have been demonstrated for mode conversion, with near-theoretical conversion efficiency. Quasi-grayscale phase masks may be created by using probabilistic amplitude masks as recording masters in the contact copy method, with the phase profiles recorded by these masks being similar to the profile recorded by an ideal grayscale amplitude masks. Probabilistic masks can be used in beam-shaping applications such as optical vortex generation, and may also be used to selectively eliminate aberrations in a system. However, because PTR samples are thick, diffraction at transition regions when using the contact copy technique can result in a degraded phase profile if there are a large number of phase transitions. For phase masks requiring no more than a few transitions though, the volume phase masks will have similar performance to traditional thin film phase masks while being suitable for use in harsher environments.

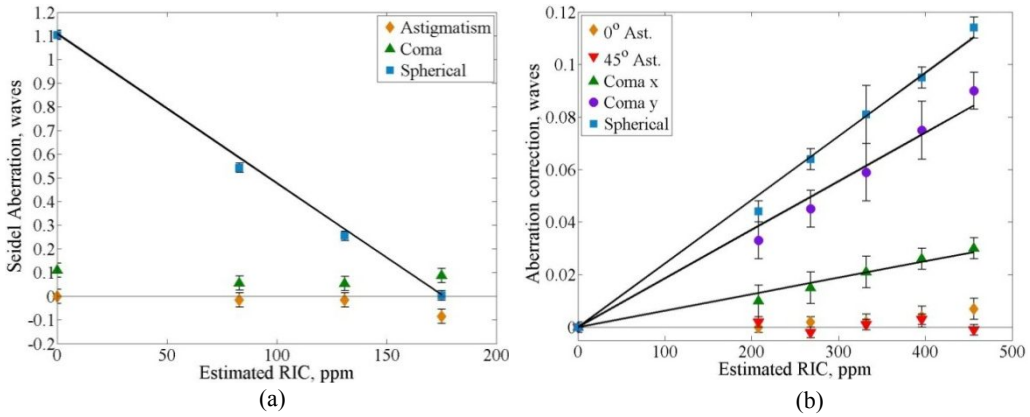

(a) (b)

Fig. 8: (Color online) Selective correction of only spherical aberration (a) and different amounts of multiple aberrations (b).

REFERENCES

[1] Castro, A., Frauel, Y., and Javidi, B., "Integral imaging with large depth of field using an asymmetric phase mask," Opt. Exp. **15**, 10266-10273 (2007).
[2] Caron, N. and Sheng, Y., "Polynomial phase masks for extending the depth of field of a microscope," App. Opt. **22**, E39-E43 (2008).
[3] Zhao, H., Li, Y., Feng, H., Xu, Z., and Li, Q., "Cubic sinusoidal phase mask: Another choice to extend the depth of field of incoherent imaging system," Opt. & Laser Tech. **42**, 561-569 (2010).
[4] Shibuya, M., "Resolution enhancement techniques for optical lithography and optical imaging theory," Opt. Review **4**, 151-160 (1997).
[5] Javidi, B. and Horner, J., "Optical pattern recognition for validation and security verification," Opt. Eng. **33**, 1752-1756 (1994).
[6] Neto, L. and Sheng, Y., "Optical implementation of image encryption using random phase encoding," Opt. Eng. **35**, 2459-2463 (1996).
[7] Cheng, C., Lin, L., Wang, C., and Chen, C., "Optical joint transform encryption using binary phase difference key mask," Phys. Review **12**, 367-371 (2005).
[8] Kumar, P., Joseph, J., and Singh, K., "Impulse attack-free four random phase mask encryption based on a 4-f optical system," App. Opt. **48**, 2356-2363 (2009).
[9] Rouan, D., Riaud, P., Boccaletti, A., Clénet, Y., and Labeyrie, A., "The four-quadrant phase-mask coronagraph. I. Principle," Pub. Ast. Soc. Pacific **112**, 1479-1486 (2000).
[10] Boccaletti, A. et al., "The four-quadrant phase-mask coronagraph. IV. First light at the Very Large Telescope," Pub. Ast. Soc. Pacific **116**, 1061-1071 (2004).
[11] Bloemhof, E., "Achromatic four-quadrant phase mask (FQPM) coronagraphy using natural beam splitter phase shifts," Opt. Exp. **13**, 10055-10060 (2005).
[12] Lumeau, J., Glebova, L., Golubkov, V., Zanotto, E. D., and Glebov, L. B., "Origin of crystallization-induced refractive index changes in photo-thermo-refractive glass," Opt. Mat. **32**, 139-146 (2009).
[13] Glebov, L. B., "Photochromic and photo-thermo-refractive (PTR) glasses," *Encyclopedia of Smart Materials*, John Wiley & Sons, NY, 770-780 (2002).
[14] Glebov, L., Flecher, E., Smirnov, V., Galvanauskas, A., and Liao, K. H., "Stretching and compression of laser pulses by means of high efficiency volume diffractive gratings with variable periods in photo-thermo-refractive glass," U.S. patent 7,424,185 B2 (2008).
[15] Sevian, A. et al., "Efficient power scaling of laser radiation by spectral beam combining," Opt. Lett. **33**, 384-386 (2008).
[16] Andrusyak, O., Smirnov, V., Venus, G., Rotar, V., and Glebov, L., "Spectral combining and coherent coupling of lasers by volume Bragg gratings," IEEE J. of Sel. Top. in Quant. Elect. **15**, 344-353 (2009).
[17] Lumeau, J., Glebov, L. B., and Smirnov, V., "Tunable narrowband filter based on a combination of Fabry–Perot etalon and volume Bragg grating," Opt. Lett. **31**, 2417-2419 (2006).
[18] Smirnov, V., et al., "Ultranarrow bandwidth moiré reflecting Bragg gratings recorded in photo-thermo-refractive glass," Opt. Lett. **35**, 592-594 (2010).
[19] Anderson, B. et al., "Forced air cooling of volume Bragg gratings for spectral beam combining," Proceedings of SPIE **8601**, 86013D (2013).
[20] Mohammed, W., Pitchumani, M., Mehta, A., and Johnson, E., "Selective excitation of the LP11 mode in step index fiber using a phase mask," Optical Engineering 45, 074602 (2006).
[21] SeGall, M. et al., "Binary volume phase masks in photo-thermo-refractive glass," Opt. Lett. **37**, 1190-1192 (2012).
[22] Efimov, O., Glebov, L., and Andre, H., "Measurement of induced refractive index in a photothermorefractive glass by a liquid-cell shearing interferometer," App. Op. **41**, 1864-1871 (2002).
[23] Ladavac, K. and Grier, D., "Microoptomechanical pumps assembled and driven by holographic optical vortex arrays," Opt. Exp. **12**, 1144-1149 (2004).
[24] Gröblacher, S., Jennewein, T., Vaziri, A., Weihs, G., and Zeilinger, A., "Experimental quantum cryptography with qutrits," New J. of Phys. **8**, 75 (2006).
[25] Yariv, A. and Yeh, P., *Photonics: Optical Electronics in Modern Communications*, Oxford University Press (2007).
[26] Rotschild, C., Zommer, S., Moed, S., Hershcovitz, O., and Lipson, S., "Adjustable spiral phase plate," App. Opt. **43**, 2397-2399 (2004).
[27] Welford, W. T., *Aberrations of Optical Systems*, Adam Hilger (IOP Publishing) , Bristol (UK) (1991).
[28] Noll, R. J., "Zernike polynomials and atmospheric turbulence," J. Opt. Soc. Am. **66**, 207-211 (1976).